

CHAPTER 3

SIZING OF THERMOSYPHON EVAPORATOR LENGTH

3.1 Introduction

For nocturnal long-wave passive cooling in this study, thermosyphon heat pipe is a tool to extract heat at its evaporator which is dipping in stored water kept in a storage tank and then heat is rejected to the surrounding at its condenser/radiator. Thus cooling water could be produced and stored in the tank. The objective of this chapter is to evaluate thermosyphon heat pipe evaporator length by experimental and then the appropriate evaporative length of the thermosyphon heat pipe could be selected. Finally, the spacing between the heat pipes evaluated by the computational fluid dynamics (CFD) will be done.

This chapter was started by setup an experiment. The evaporator length of the thermosyphon heat pipe was varied then the water temperature at each time step was measured so that we could calculate the rate of heat transfer at each time step by Equation 3.1. The surface temperature of thermosyphon heat pipe was collected so

that the averaged convective heat transfer coefficient (\bar{h}) was carried out by Equation 3.2. The averaged convective heat transfer coefficient was substituted as a CFD input

to analyze the spacing between thermosyphon heat pipes for the prototype scale. The averaged convective heat transfer coefficient was also transformed into Nusselt number which is one of the designed parameter for the prototype scale. Nusselt

number, on its definition, can lead to averaged convective heat transfer coefficient which can define the amount of the thermosyphon heat pipe at the final. The designed methodology was shown in Figure 3.1.

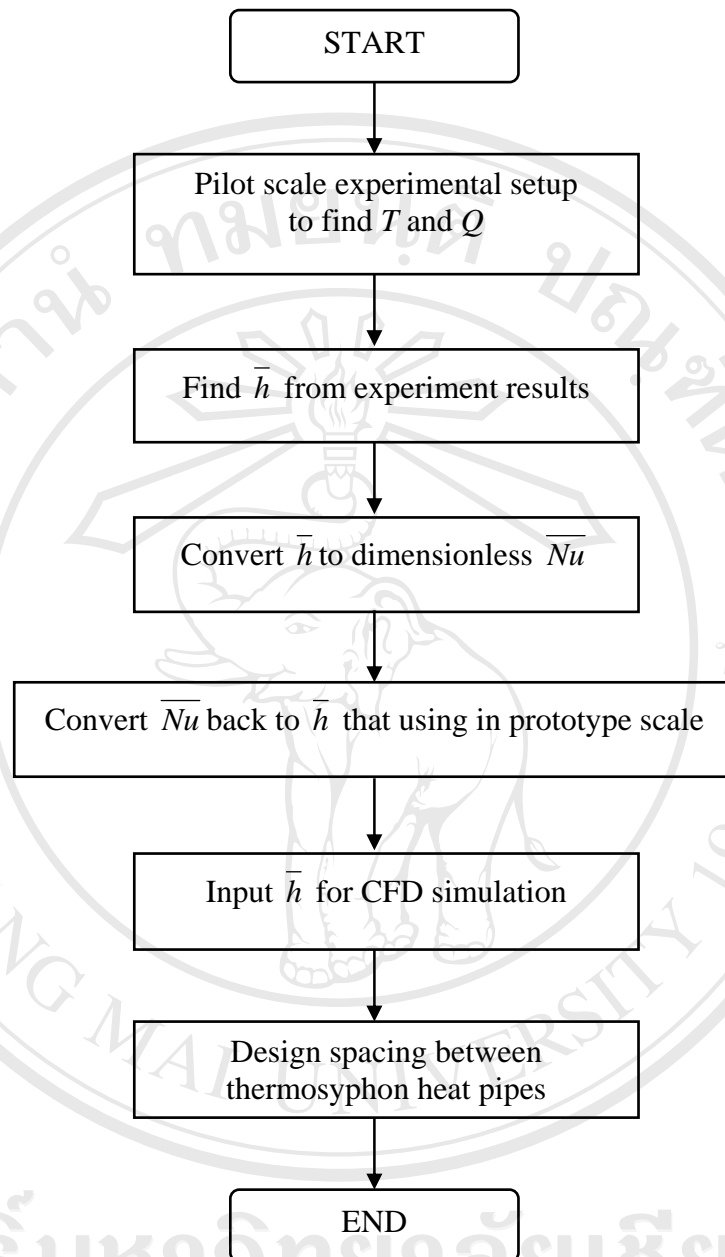


Figure 3.1 Flow chart of the design concept.

3.2 Experimental Setup

In our experiments, there were three copper thermosyphon heat pipes of which the evaporator sections were dipped into three well-insulated vessels each contained 3.5 L of water. The thermosyphon heat pipes had the same outside diameter of 19.05 mm and each contained R-134a at 0.6 filling ratio. The schematic sketch of the experimental setup was shown in Figure 3.2. The condenser length (L_c) and the adiabatic length (L_a) of each thermosyphon heat pipe were set to be 0.45 and 0.10 m, respectively. Different evaporative lengths (L_e), 0.45, 0.30 and 0.15 m, were used to extract heat from water in the vessels so that the overall length of each thermosyphon heat pipe was different. The depth of water storage vessel (L) was 0.45 m. Then the L_e/L ratios of the three thermosyphon heat pipes were 1.00, 0.67 and 0.33 respectively. The initial water temperature in each vessel was at 27.0 °C. The condenser parts of the thermosyphons were in a cool water bath which was maintained uniformly at 10.0 °C.

Fluid and surface temperature were measured by temperature sensors as shown in Figure 3.3, calibrated individually so that the differential error of measurement was less than ± 0.1 °C. All data were transferred to a 16 channel data-logger and collected every 600 seconds. The fluid and the surface temperatures were multi-point measurements, so the averaged value could be detected. Figure 3.4 shows the attaching method of the temperature sensors.

The water temperature data from the experiments were used to calculate the rate of rejected heat by the thermosyphon heat pipe by

$$\dot{Q} = \frac{m_w C_{p(w)} (T_w^t - T_w^{t+\Delta t})}{\Delta t}, \quad (3.1)$$

where \dot{Q} is the rate of rejected heat [W],

m_w is the mass of water in studied time step [kg],

$C_{p(w)}$ is the heat capacity of water [$\text{J kg}^{-1} \text{K}^{-1}$],

T_w is the water temperature [K],

Δt is the time interval [s].

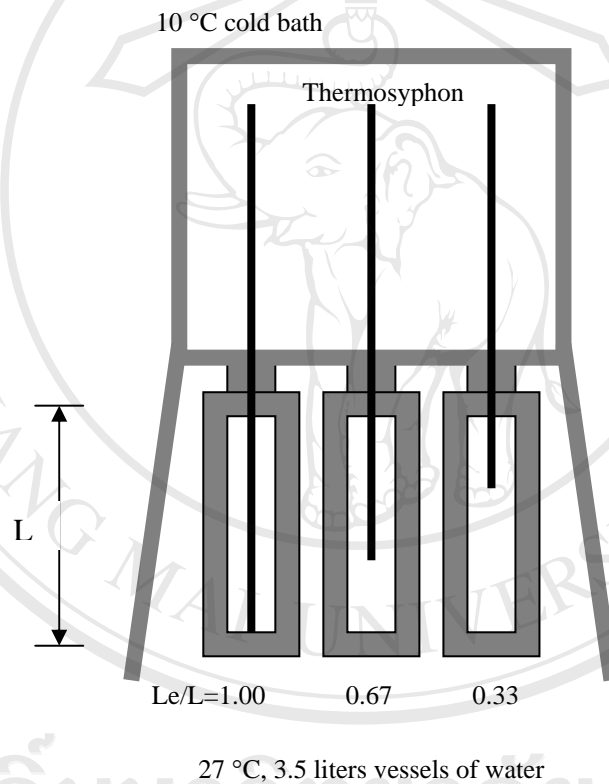


Figure 3.2 Schematic drawing of the experimental setup.

The rate of rejected heat from each time interval was used to calculate the averaged combined convective and radiative heat transfer coefficients at each thermosyphon heat pipe as

$$\bar{h} = \frac{\dot{Q}}{A(T_w - T_s)}, \quad (3.2)$$

where \bar{h} is the averaged convective heat transfer coefficients [$\text{W m}^{-2} \text{K}^{-1}$],

A is thermosyphon heat pipe surface area [m^2],

T_s is the thermosyphon heat pipe surface temperature [K].

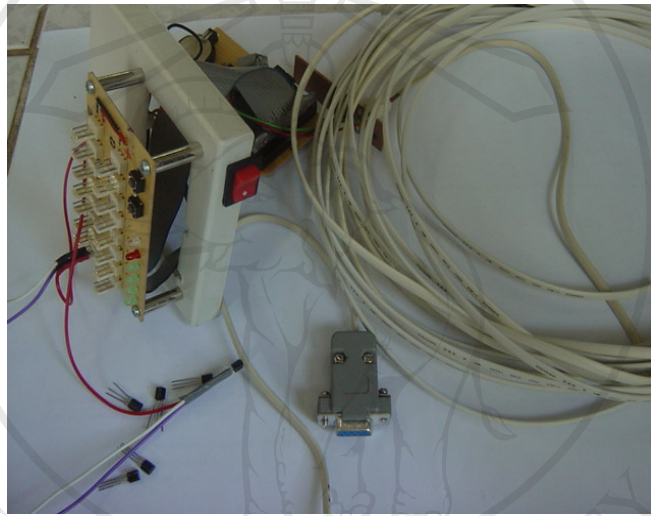


Figure 3.3 Temperature sensors with 16 channel data logger, ± 0.1 °C in accuracy.

The averaged convective heat transfer coefficient of the entire experiment would be an input for the CFD simulation.

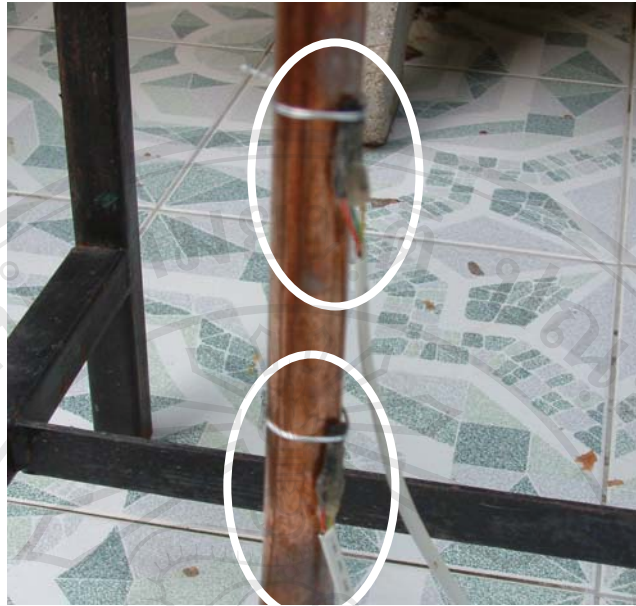


Figure 3.4 Attaching the sensors with the thermosyphon heat pipe by chromium wire before coating with silicone sealant.

The experimental results of water temperature and rejected heat between thermosyphon heat pipe, having $L_e/L_c = 1.00$, 0.67 and 0.33 were shown in Figures 3.5 and 3.6, respectively. Due to the larger evaporative part surface area, the $L_e/L_c = 1.00$ thermosyphon heat pipe unit could reject heat from the system more than the $L_e/L_c = 0.67$ and $L_e/L_c = 0.33$ by 19.4% and 28.7% , respectively. This condition also gave the lowest water temperature. Although this case took more investment on materials when compared with the case $L_e/L_c = 0.67$ and $L_e/L_c = 0.33$, around 33.3% and 66.6% , respectively, we also selected this case to investigate the prototype model because of its cooling performance.

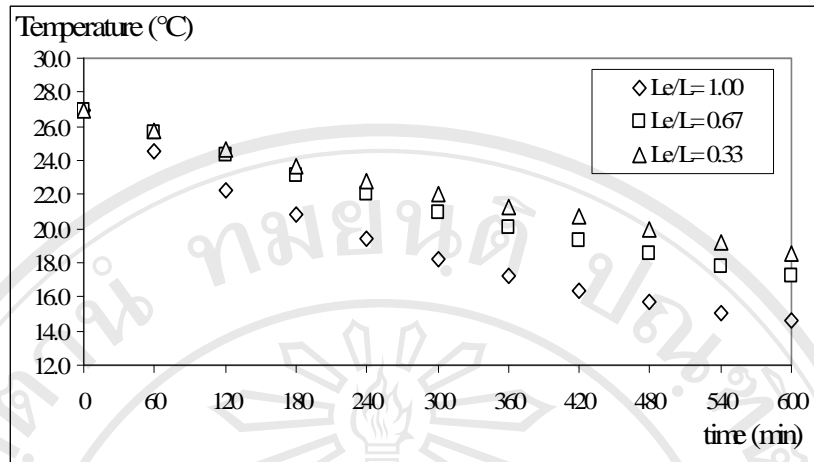


Figure 3.5 The experimental result of water temperature between $L_e/L = 1.00, 0.67$ and 0.33 studied cases.

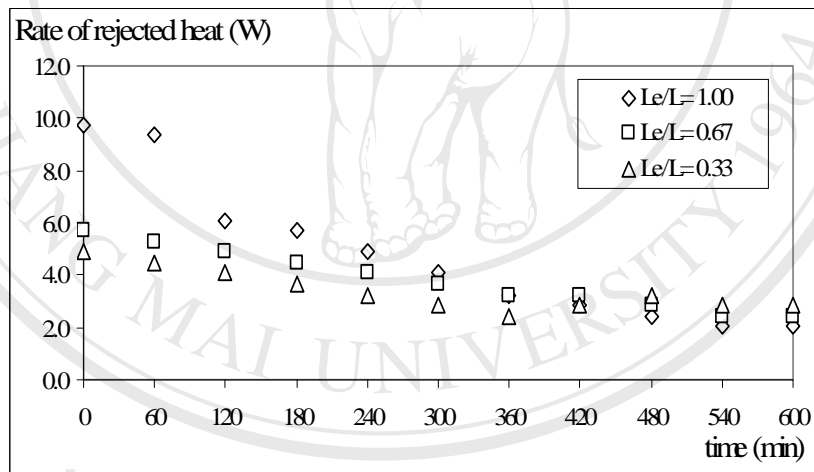


Figure 3.6 The experimental result of rate of rejected heat between $L_e/L = 1.00, 0.67$ and 0.33 studied cases.

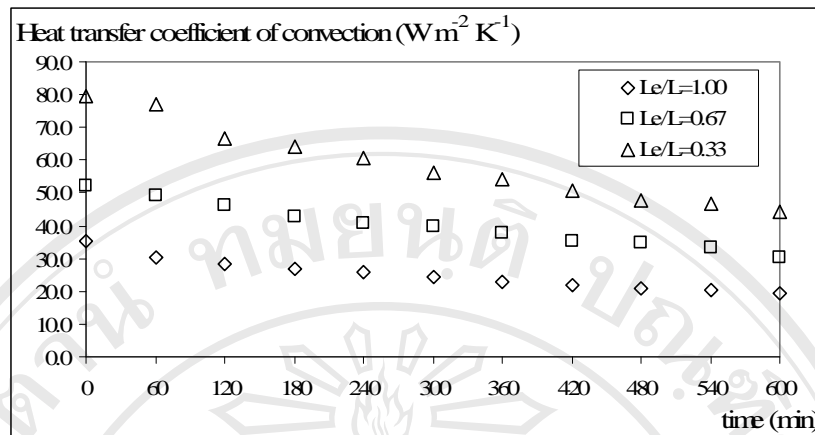


Figure 3.7 The averaged convective heat transfer coefficient for each L_e/L .

As shown in Figure 3.7, the averaged convective heat transfer coefficient (\bar{h}) of each case gradually went down along with the time because the fluid around the thermosyphon evaporator moved slower due to the reduction of its driving force, the different temperature ($T_w - T_s$). The averaged convective heat transfer coefficient was evaluated by Equation 3.2 and found to be around 25.2, 40.2 and 58.9 $\text{W m}^{-2} \text{K}^{-1}$ or Nusselt Number (\overline{Nu}) 18.9, 20.1 and 14.7 ($\overline{Nu} = \frac{\bar{h}L}{k}$) for the cases of $L_e/L = 1.00$, 0.67 and 0.33, respectively. The heat transfer coefficient of each case was not the same. The evaporator lengths of the dipped thermosyphon heat pipes had directly effect on their heat transfer coefficient because the moving fluid in their boundary layer was accelerated by gravity and had larger velocity along the pipe length. The ratio $L_e/L = 1.00$ gave the largest heat transfer and selected for prototype scale. Then CFD simulation by CFD package was done for verify the spacing between thermosyphon heat pipe in the prototype scale. The averaged convective heat transfer coefficients above were worked as an input data at the convective boundary conditions for the CFD simulation, described in the next section. In the prototype

scale, the 1.0 m³ water storage tank was selected to be a thermal storage in which it was large enough to absorb heat from a 9.0 m² tested room

The rejected heat from one thermosyphon heat pipe could be found by Equation 2.1 to 2.19, some calculation parameters have shown in Table 3.1.

Table 3.1 The calculation parameters for the experimental system design.

Description	Value	Unit
Outside diameter	19.05	mm
Tube thickness	0.75	mm
Evaporator length	1.5	m
Adiabatic length	0.2	m
Condenser length	1.5	m
Thermal conductivity of copper tube	400.0	W m ⁻¹ K ⁻¹
Working Fluid	R-134a	
Filling ratio	0.6	
Heat source initial temperature	27.0	°C
Heat sink temperature	10.0	°C
Covective heat transfer coefficient at evaporator	7	W m ⁻² K ⁻¹
Covective heat transfer coefficient at condenser	7	W m ⁻² K ⁻¹

The calculated result by Equation 2.1 to 2.19 showed that for one thermosyphon heat pipe, it could reject heat around 4.5 watts. The 48 thermosyphon heat pipes, which could reject heat around 216 watts, were installed in the rectangular storage tank as shown in Figure 3.8. This configuration can reduce the 1.0 m³ of water temperature at least 2.0 °C down each night.

The dimension of the 1.0 m³ tank was controlled by its strength limit and was found to be 3.3 m x 1.5 m x 0.2 m.

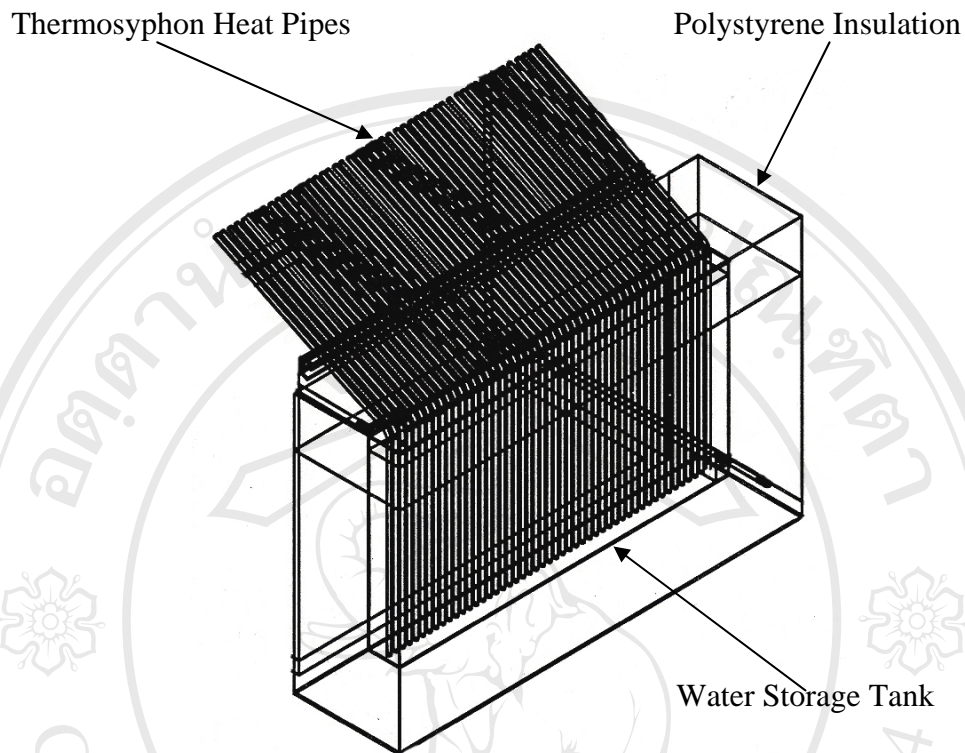


Figure 3.8 The 1.0 m³ water storage tank with 48 thermosyphon heat pipe.

3.3 Simulation Setup

Finite volume solution was used. This approach implied that the discrete equations were formulated by evaluating and integrating the fluxes across the faces that surrounded each control volume. This method allowed the solutions for incompressible problems where pressure was loosely coupled to density.

Further, the Navier-Stokes equations form a vector continuity equation describing the conservation of linear momentum. The Navier-Stokes equations are nonlinear partial differential equations in almost any real situation.

Navier-Stokes equations (2008) stated that the vast majority of work on the Navier-Stokes equations is done under an incompressible flow assumption for

Newtonian fluids. Taking the incompressible flow assumption into account and assuming constant viscosity, the Navier-Stokes equations will read in vector form as

$$\rho \left(\frac{\partial \mathbf{v}}{\partial t} + \mathbf{v} \cdot \nabla \mathbf{v} \right) = -\nabla p + \mu \nabla^2 \mathbf{v} + \mathbf{f}, \quad (3.3)$$

It's well worth observing the meaning of each term

$\rho \left(\frac{\partial \mathbf{v}}{\partial t} + \mathbf{v} \cdot \nabla \mathbf{v} \right)$	is inertia term,
$\frac{\partial \mathbf{v}}{\partial t}$	is unsteady acceleration term,
$\mathbf{v} \cdot \nabla \mathbf{v}$	is convective acceleration term,
∇p	is pressure gradient term,
$\mu \nabla^2 \mathbf{v}$	is viscosity term,
\mathbf{f}	is other body forces such as gravity or centrifugal force term.

Note that only the convective terms are nonlinear for incompressible Newtonian flow. Under the incompressible assumption, density is a constant and the term $\nabla \cdot \mathbf{v}$ can be set to be zero.

The Cartesian equations follow directly from the vector equation above. Obtaining equations in other coordinate systems will require a change of variables.

Writing the vector equation explicitly in Cartesian coordinates as

$$\rho \left(\frac{\partial u}{\partial t} + u \frac{\partial u}{\partial x} + v \frac{\partial u}{\partial y} + w \frac{\partial u}{\partial z} \right) = -\frac{\partial p}{\partial x} + \mu \left(\frac{\partial^2 u}{\partial x^2} + \frac{\partial^2 u}{\partial y^2} + \frac{\partial^2 u}{\partial z^2} \right) + \rho g_x, \quad (3.4)$$

$$\rho \left(\frac{\partial v}{\partial t} + u \frac{\partial v}{\partial x} + v \frac{\partial v}{\partial y} + w \frac{\partial v}{\partial z} \right) = -\frac{\partial p}{\partial y} + \mu \left(\frac{\partial^2 v}{\partial x^2} + \frac{\partial^2 v}{\partial y^2} + \frac{\partial^2 v}{\partial z^2} \right) + \rho g_y, \quad (3.5)$$

$$\rho \left(\frac{\partial w}{\partial t} + u \frac{\partial w}{\partial x} + v \frac{\partial w}{\partial y} + w \frac{\partial w}{\partial z} \right) = - \frac{\partial p}{\partial z} + \mu \left(\frac{\partial^2 w}{\partial x^2} + \frac{\partial^2 w}{\partial y^2} + \frac{\partial^2 w}{\partial z^2} \right) + \rho g_z. \quad (3.6)$$

Note that gravity has been accounted for as a body force, and the values of g_x , g_y and g_z will depend on the orientation of gravity with respect to the chosen set of coordinates. The continuity equation reads

$$\frac{\partial u}{\partial x} + \frac{\partial v}{\partial y} + \frac{\partial w}{\partial z} = 0, \quad (3.7)$$

when u is the velocity component in x direction,
 v is the velocity component in y direction,
 w is the velocity component in z direction.

The energy equation can be still derived by starting with the Navier-Stokes equation as mention above and be denoted that

$$\begin{aligned} \frac{\partial}{\partial t} \left[\rho \left(e + \frac{V^2}{2} \right) \right] + \nabla \cdot \left[\rho \left(e + \frac{V^2}{2} \right) \mathbf{v} \right] &= \rho \dot{q} + \frac{\partial}{\partial x} \left(k \frac{\partial T}{\partial x} \right) + \frac{\partial}{\partial y} \left(k \frac{\partial T}{\partial y} \right) \\ &+ \frac{\partial}{\partial z} \left(k \frac{\partial T}{\partial z} \right) - \frac{\partial (up)}{\partial x} - \frac{\partial (vp)}{\partial y} - \frac{\partial (wp)}{\partial z} + \frac{\partial (u\tau_{xx})}{\partial x} \\ &+ \frac{\partial (u\tau_{yx})}{\partial y} + \frac{\partial (u\tau_{zx})}{\partial z} + \frac{\partial (v\tau_{xy})}{\partial x} + \frac{\partial (v\tau_{yy})}{\partial y} + \frac{\partial (v\tau_{zy})}{\partial z} \\ &+ \frac{\partial (w\tau_{xz})}{\partial x} + \frac{\partial (w\tau_{yz})}{\partial y} + \frac{\partial (w\tau_{zz})}{\partial z} + \rho \mathbf{f} \cdot \mathbf{v}, \end{aligned} \quad (3.8)$$

when e is internal energy per unit mass term,

$\frac{V^2}{2}$ is the kinetic energy due to fluid element translational motion term.

The CFD simulation was done to evaluate the temperature profile between the thermosyphon heat pipe whether it closed enough to maintain the uniform water temperature.

At this time, the computation domains were water in the storage tank between thermosyphon heat pipes which were divided into 4500 grids. As shown in Figure 3.9. The three thermosyphon heat pipes were selected as parameters for all 48 pipes. The convective boundary conditions ($\bar{h}=\text{constant}$) were set at the thermosyphon surfaces. The averaged convective heat transfer coefficients from an experiment were substituted as an input data in the CFD simulation. The adiabatic boundary conditions were set around the computation domains. The starting water temperature was set to be 27°C. The calculated outputs were vector flow fields and also fluid temperatures at each time steps.

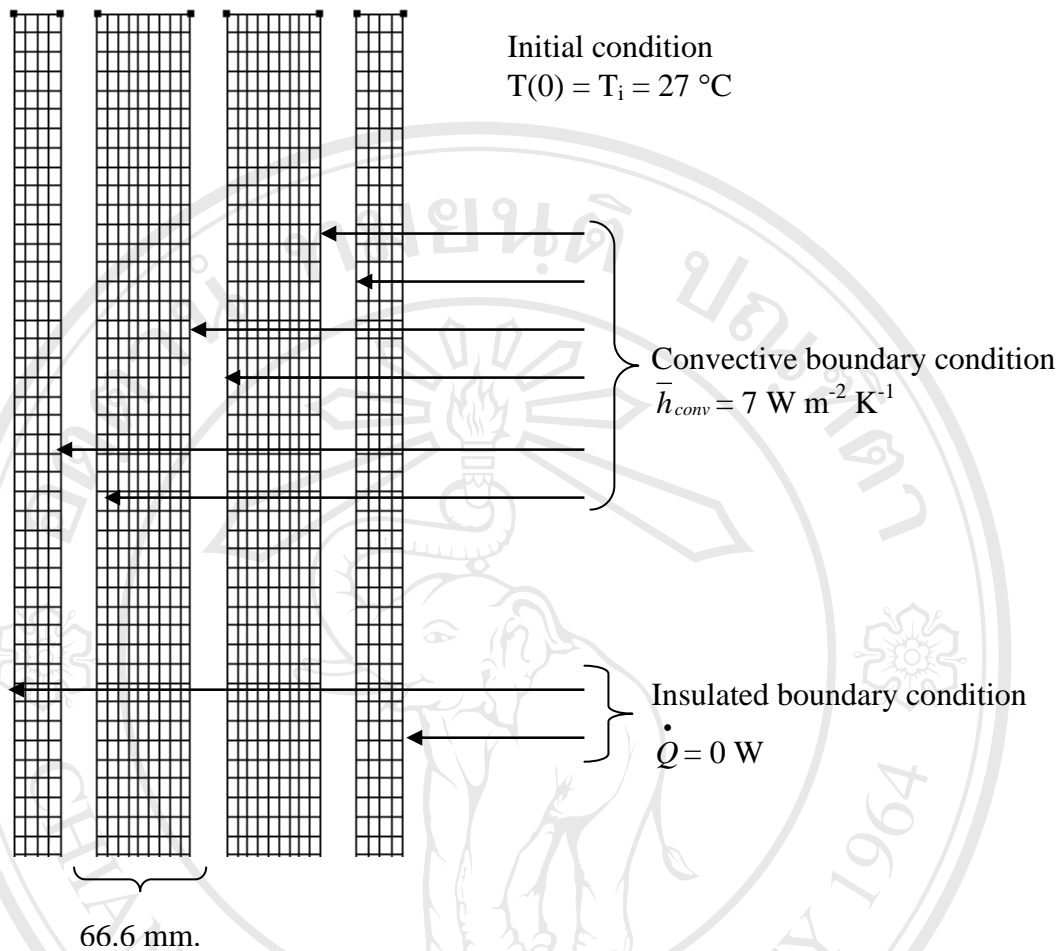


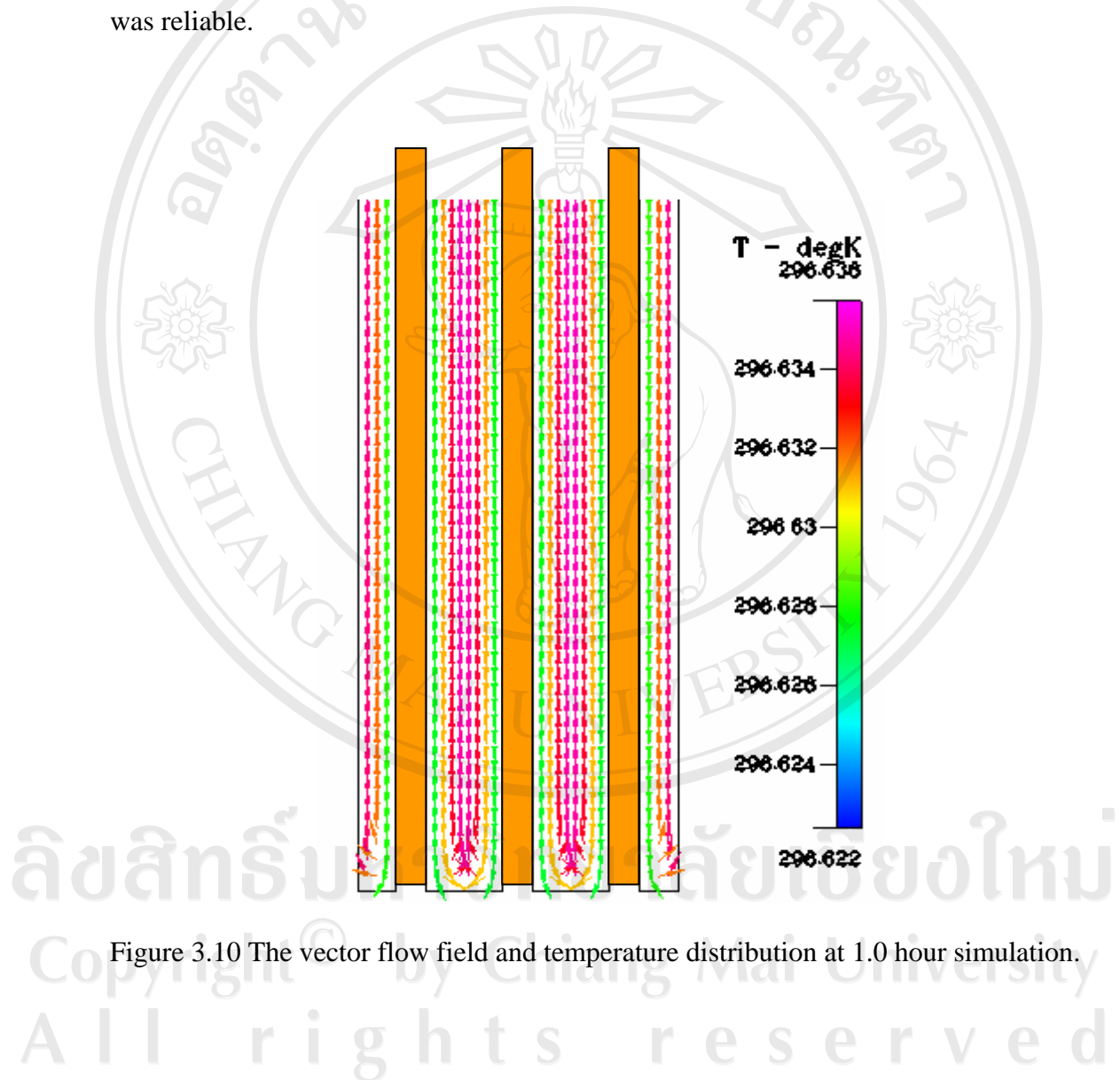
Figure 3.9 The computational domain of $L_c/L = 1.00$ by structure grid. The initial and boundary condition applied at the computation domain.

In this research, the simulation program was prepared by the CFD package program, which based on finite volume method.

3.4 Results and Discussion

The simulated results at 1.0 hour and 12.0 hours of simulation have shown in Figure 3.10 and 3.11, respectively. The vector flow field and temperature distribution at 1.0 hour was verified that the 66.6 mm spaces between thermosyphon heat pipes

were close enough to maintain water temperature between them, was not to fluctuate over 0.1 °C, when that of 12.0 hours was not to fluctuate over 0.01 °C. The fluctuation in temperature between each thermosyphon heat pipe was not over than the accuracy of the temperature sensors in which ± 0.1 °C so that the recorded data was reliable.



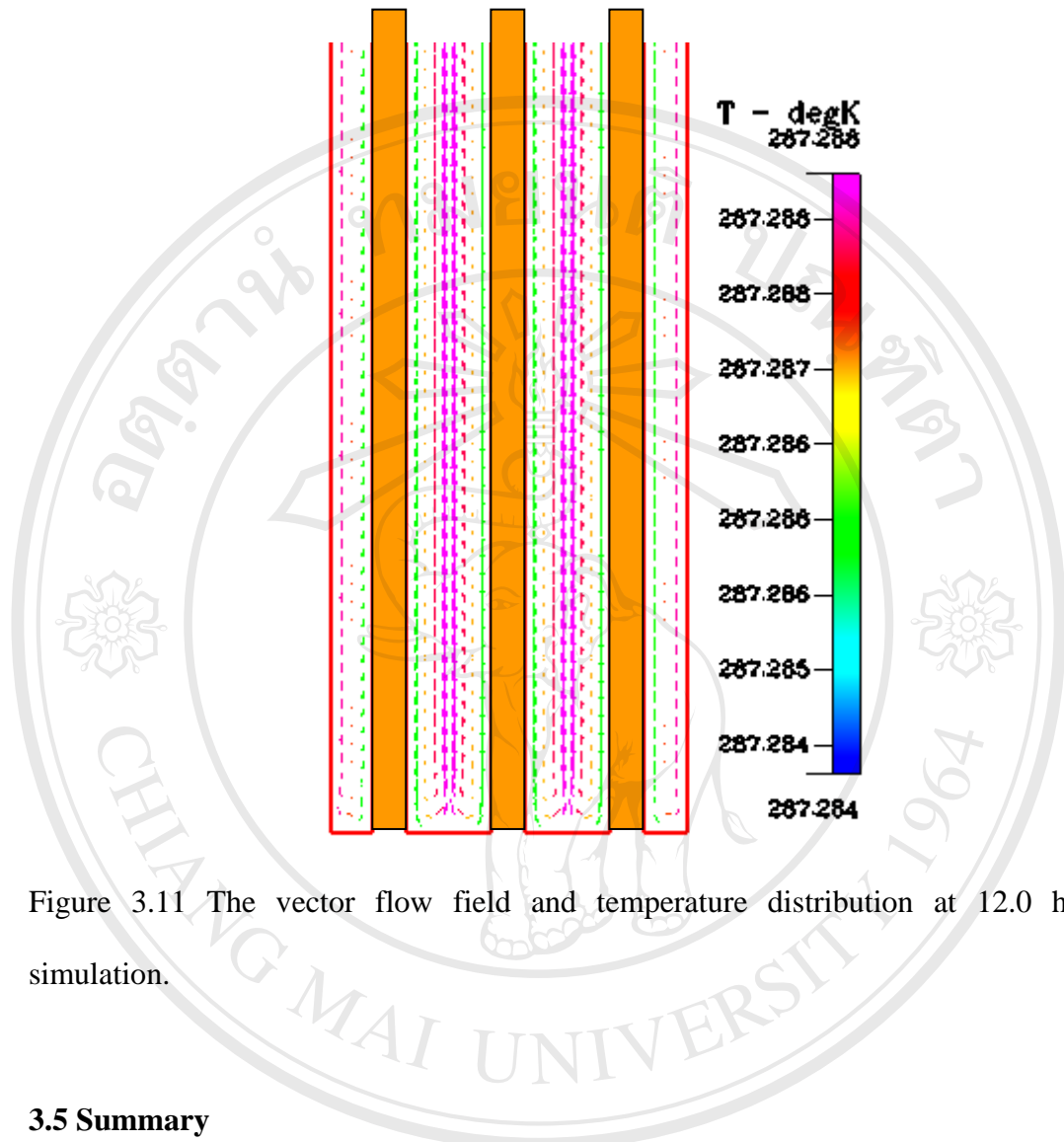
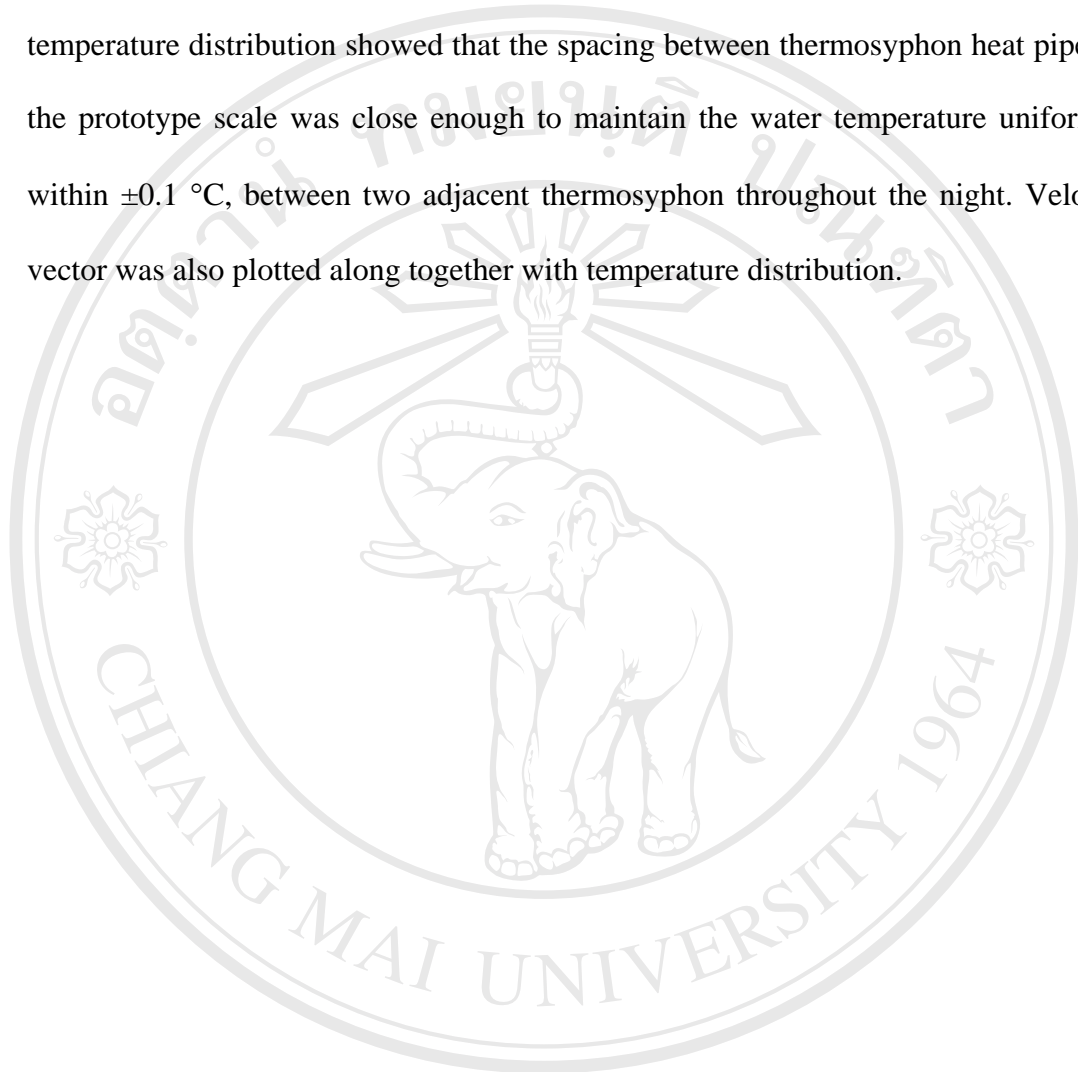


Figure 3.11 The vector flow field and temperature distribution at 12.0 hours simulation.

3.5 Summary

This study showed the effect of the evaporative length on the heat transfer of thermosyphon heat pipe when dipped in the water storage. Due to the larger evaporator surface area, the $L_e/L = 1.00$ thermosyphon heat pipe unit could reject heat from the system more than the $L_e/L = 0.67$ and $L_e/L = 0.33$ by 19.4% and 28.7%, respectively. This condition also gave the lowest water temperature. The ratio $L_e/L = 1.00$ was selected for prototype scale. Then CFD simulation by CFD package was done to verify the spacing between thermosyphon heat pipes in the prototype scale.

The averaged convective heat transfer coefficients from an experiment were worked as an input data at the convective boundary conditions for the CFD simulation. The temperature distribution showed that the spacing between thermosyphon heat pipes in the prototype scale was close enough to maintain the water temperature uniformly, within ± 0.1 °C, between two adjacent thermosyphon throughout the night. Velocity vector was also plotted along together with temperature distribution.



ลิขสิทธิ์มหาวิทยาลัยเชียงใหม่

Copyright© by Chiang Mai University

All rights reserved